Hydro-mechanical analysis during fluid injection into a geologic formation and implications for CO_2 geologic storage

Analyse hydro-mécanique lors de l'injection de fluide dans une formation géologique et implications pour le stockage géologique du CO_2

Seunghee Kim
Department of Civil Engineering, University of Nebraska-Lincoln, USA, seunghee.kim@unl.edu

Seyyed A. Hosseini
Bureau of Economic Geology, The University of Texas at Austin, USA, seyyed.hosseini@beg.utexas.edu

ABSTRACT: Success of CO_2 geologic storage is contingent on the geomechanical safety of a storage site. Pore pressure is expected to increase during fluid injection, so precisely predicting the resulting stress path is key to evaluate a geomechanical failure risk. Recent studies support the observation that total stresses change in every direction as the fluid injection disturbs the pore-pressure field and causes displacements and the redistribution of stresses. In this regard, we conducted numerical simulations that couple fluid flow in porous media with solid mechanics to investigate the ratios of total stress changes to pore-pressure change $\Delta\sigma/\Delta P$ at different times and locations during the fluid injection. These numerical experiments provided salient observations such as: the asymptotic value of $\Delta\sigma_r/\Delta P$ at the interface between the injection layer and caprock is greater than that in the middle of injection layer by 10~15%; and a broad area at the interface converges to $\Delta\sigma_z/\Delta P\approx(\alpha/2)(1\text{-}2\nu)/(1\text{-}\nu)$, while the middle line converges to $\Delta\sigma_z/\Delta P\approx0$. Unlike the traditional approach or the simplified poroelastic analysis, accurate reflection of the stress/pore-pressure change ratios can provide a reliable estimate of the effective stresses and thus the maximum sustainable pressure limit.

RÉSUMÉ : Le succès du stockage géologique du CO_2 dépend de la sécurité géomécanique d'un site de stockage. On s'attend à ce que la pression de pores augmente pendant l'injection de fluide, de sorte qu'une prédiction précise du chemin de contrainte résultant est une clé pour évaluer un risque d'échec géomécanique. Des études récentes soutiennent l'observation que les contraintes totales changent dans tous les sens puisque l'injection de fluide perturbe le champ de pression interstitielle et provoque des déplacements et la redistribution des contraintes. À cet égard, nous avons effectué des simulations numériques qui couplent l'écoulement de fluide dans des milieux poreux avec une mécanique des solides pour étudier les rapports entre les changements de contraintes totales et la variation de pression poreuse $\Delta\sigma/\Delta P$ à différents moments et endroits pendant l'injection de fluide. Ces expériences numériques ont fourni des observations saillantes telles que: la valeur asymptotique de $\Delta\sigma_r/\Delta P$ à l'interface entre la couche d'injection et le caprock est supérieure à celle au milieu de la couche d'injection de 10~15%; Et une large zone à l'interface converge vers $\Delta\sigma_z/\Delta P\approx(\alpha/2)(1\text{-}2\nu)/(1\text{-}\nu)$, alors que la ligne médiane converge vers $\Delta\sigma_z/\Delta P\approx0$. Contrairement à l'approche traditionnelle ou à l'analyse poroélastique simplifiée, une réflexion précise des rapports de contrainte/pression de pore-pression peut fournir une estimation fiable des contraintes efficaces et donc de la limite de pression maximale durable.

KEYWORDS: Poroelasticity, pore-pressure/stress change ratio, induced seismicity, and CO_2 geologic storage.

1 INTRODUCTION

Carbon capture, utilization and storage (CCUS) has been actively studied in the last decade because this operation might potentially constitute a bridge from a fossil-fuel-dependent system to a next system with a dominance of renewable energy sources (Socolow and Pacala, 2006). Geologic carbon sequestration involves injecting carbon dioxide (CO_2), which is captured from an emission source and transported to a storage site, into a geologic formation that is typically deeper than 800 m (IPCC, 2005). Injecting CO_2 into a geologic formation is expected to cause changes in total stresses as the pore pressure builds up during the operation (Kim and Hosseini, 2015, Preisig and Prévost, 2011, Rutqvist, 2012, Vilarrasa et al., 2013). Therefore, accounting for both pore-pressure buildup and ensuing stress changes to predict stress paths is key for judging as to how the stress state approaches geomechanical failure criteria and how the maximum sustainable pressure limit should be set accordingly. But unlike the horizontal stress change, the vertical stress change has been neglected frequently due to the presence of a free surface. However, many recent studies ascertain that total stresses change both vertically and horizontally as fluid extraction/injection disturbs the pore-pressure field and causes displacements as well as the redistribution of stresses (Altmann et al., 2010, Safari et al., 2013, Schoenball et al., 2010). In this manuscript, we present several numerical-simulation results that shed light on the spatio-temporal evolution of the ratios of stress/pore-pressure changes in both horizontal and vertical directions. On the basis of observations from these numerical simulations, we discuss implications of the pore-pressure/stress coupling effect for determining consequent changes in effective stresses and maximum sustainable pressure limit.

2 NUMERICAL SIMULATION

2 .1 *Simulation method*

The analytical solution for the ratio of stress/pore-pressure change $\Delta\sigma/\Delta P$ is valid for point injection into a homogeneous infinite isotropic medium as follows (Altmann et al., 2010);

$$\frac{\Delta\sigma_{ij}(x,t)}{\Delta P(x,t)}=\frac{\alpha(1-2\nu)\{\delta_{ij}[erfc(1/2\xi)-(2/\xi^2)ig(\xi)]+(x_i x_j/r^2)[erfc(1/2\xi)+(6/\xi^2)ig(\xi)]\}}{2(1-\nu)erfc(1/2\xi)} \quad (1)$$

where α is Biot's coefficient, ν is Poisson's ratio, δ_{ij} is the Kronecker delta, $erfc(z)=1-erf(z)$ is the complementary error function, and $\xi=r/(ct)^{1/2}$ is Boltzmann variable (r=radial distance; c=hydraulic diffusivity; t=time).

In real applications, however, property contrasts exist between an injection layer and surrounding strata. The analytic solution is good for the spherical domain, but the property contrasts dictate the domain rather close to the cylindrical one. Hydraulic boundary conditions may also affect the evolution of $\Delta\sigma/\Delta P$ during fluid injection. We used the commercial software COMSOL to investigate the spatio-temporal evolution of $\Delta\sigma/\Delta P$ during fluid injection into an injection layer. The single-phase flow condition is employed to focus on the poroelastic effect. Note that two-phase flow condition should be considered if the main purpose of numerical simulation is to examine pore-pressure buildup driven by CO_2 injection. We also assumed isothermal condition (ΔT=0) to rule out the thermal stress effect. In COMSOL, we coupled physical models for the fluid flow in porous media with solid mechanics: change in fluid content is fully coupled with strains and stresses during the numerical simulation. Refer to Kim and Hosseini (2015) for the detailed information about the simulation method.

2 .2 *Simulation model and parameters*

Unlike the geometry for the analytical solution, we intended to investigate spatio-temporal variation of $\Delta\sigma/\Delta P$ during fluid injection when the environment is neither infinite nor homogeneous. In addition, line injection is more realistic than the point injection. With this purpose, we built the simplified simulation model as shown in Figure 1. The left end of the model is an axis of symmetry. A constant fluid-injection rate is imposed on the left end of the injection layer during the numerical simulation while gravity is turned off. Depth to the top of injection layer, the only layer with a high permeability value, is 1000 m. Thickness of the injection zone is set to 100 m. With this model, we conducted numerical simulations for various conditions: that is, many numerical "experiments" were carried out.

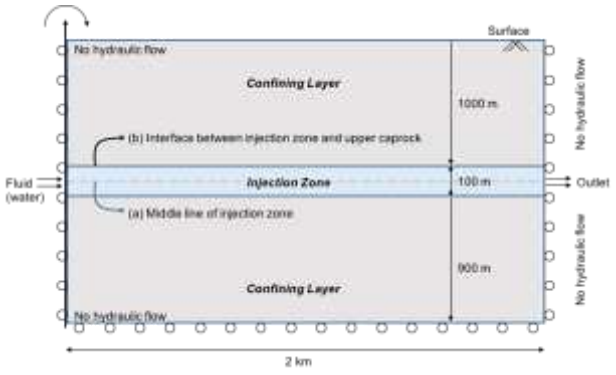

Figure 1. Simulation model for numerical experiments in this study: Geometry and the lines of interest (center line of injection layer and interface between injection layer and upper caprock).

The right end of the injection layer is set either as a fluid outlet or closed boundary to investigate the impact of hydraulic boundary conditions. The top and bottom ends of the model are set as no flow boundaries. In terms of mechanical boundary conditions, rollers (i.e., only translational displacement is allowed) are imposed on the left and right ends and the bottom of the model. The top surface is free to move. The radial and vertical boundaries are 2 km away from left and top, respectively, to reflect the finite boundary condition. The upper caprock that overlies the injection layer is assigned a permeability of either k_{cap}=1 nd ($\approx 10^{-21}$m^2, almost impermeable) or k_{cap}=1 μd ($\approx 10^{-18}$ m^2, somewhat permeable, but much less permeable than the injection layer), and the other layer below the injection zone is fixed with k=1 nd. Table 1 summarizes all parameter values applied for various realizations during the numerical study.

3 NUMERICAL EXPERIMENT: RESULTS

We herein present numerical simulation results for different hydraulic boundary and caprock permeability conditions. In particular, we focus on the evolution of the ratio of change in total radial stress to change in pore-pressure $\Delta\sigma_r/\Delta P$ and the ratio of change in total vertical stress to change in pore-pressure $\Delta\sigma_z/\Delta P$. Compression is positive for stresses as in traditional geotechnical engineering. We also primarily focus on two lines of interest: (a) *the middle* line of the injection layer and (b) *the interface* between the injection layer and the upper caprock (Figure 1).

Table 1. Input parameters for numerical simulations.

Property	Symbol	Value	
		Injection zone	Confining layers
Young's modulus	E	30 GPa	
Poisson's ratio	ν	0.3	
Dry bulk density	ρ_d	2250 km/m^3	
Porosity	ϕ	0.25	
Biot's coefficient	α	1	
Bulk modulus of fluid	K_f	2.2 GPa	
Density of fluid	ρ_f	1000 kg/m^3	
Viscosity of fluid	η	0.001 Pa·s	
Permeability	k	100 md	1 μd or 1 nd
Injection rate	Q	1 kg/s	
Radius of the injection well	r_w	0.1 m	
Thickness of the injection well	T_{IZ}	100 m	
Depth of injection zone	D_{IZ}	1000 m	
Simulation (injection) time	t_{simul}	365 days (1 year)	

3 .1 *Hydraulic Boundary Condition*

Figure 2 shows simulation results when the hydraulic boundary of the injection layer (right end) is open for flow. Ratio $\Delta\sigma_r/\Delta P$ increases with distance away from the injection well (Figures 2-a and b): it is because the pressure change ΔP diminishes toward zero faster than the total stress change $\Delta\sigma_r$. While the propagation of excess pore pressure depends on the intrinsic permeability of the porous media, change in stress travels via deformation of the rock skeleton (Rutqvist, 2012). Thus, the large value of $\Delta\sigma_r/\Delta P$ when the pore-pressure buildup is insignificant, i.e., ΔP<1 MPa, is indeed negligible. As injection time elapses, broader area of the injection layer converges to $\Delta\sigma_r/\Delta P=\alpha(1-2\nu)/(1-\nu)$ as shown in Figure 2-a. We also observed that the asymptotic value of $\Delta\sigma_r/\Delta P$ is greater at the *interface* between the injection layer and the upper caprock (line *b* in Figure 1) than along the *middle* of the injection layer (line *a* in Figure 1). Fluid flow into the caprock is hindered due to the low permeability of caprock, so the excess pressure at the interface is transmitted via rock skeleton, not via the fluid flow as in the case inside of the injection layer. This rationale can explain the higher value of stress/pore-pressure change ratio $\Delta\sigma_r/\Delta P$ at the *interface* than at the *middle*.

On the other hand, the ratio $\Delta\sigma_z/\Delta P$ decreases with distance away from the injection well; this ratio even converts from positive (compressive) to negative (tensile) values (Figure 2-c). As in the case of radial stress, $\Delta\sigma_z/\Delta P$ is greater at the *interface* than at the *middle* (see Figures 2-c and d). Moreover, a broad area at the interface converges to the asymptotic value $\Delta\sigma_z/\Delta P\approx(\alpha/2)(1-2\nu)/(1-\nu)$, whereas the middle line converges to $\Delta\sigma_z/\Delta P\approx 0$. Note that the expansion of pressurized injection layer is resisted by the rigidity of the overlying caprock (Rutqvist et al., 2007), as well as the flow of pressurized fluid into the caprock is hindered. This combination results in the compression at the interface (and the lower part of the caprock) as fluid is injected (Segall and Fitzgerald, 1998, Vilarrasa et al.,

2013). Therefore, neglecting the vertical stress change is valid only for the inside of the injection layer. Furthermore, note that the spatio-temporal evolution of $\Delta\sigma/\Delta P$ becomes minute after ~10 days of fluid injection, exhibiting a rapid convergence to an asymptote curve.

Next, we switched the hydraulic boundary condition at the end of the injection layer from open to closed. Asymptote curves become flat accordingly (compare Figures 2 and 3). Specifically, the entire area converges to the corresponding asymptotic values (i.e., $\Delta\sigma_r/\Delta P \approx \alpha(1-2\nu)/(1-\nu)$ at the *middle*, and $\Delta\sigma_z/\Delta P \approx (\alpha/2)(1-2\nu)/(1-\nu)$ at the *interface*) as a result of the closed hydraulic boundary. The no-flow condition permits the pore-pressure buildup to accumulate at the boundary similar to that the stress increases accumulate. Consequently, the entire length attains the same value of $\Delta\sigma/\Delta P$ after a certain elapse of injection time (~10 days for this simulation model).

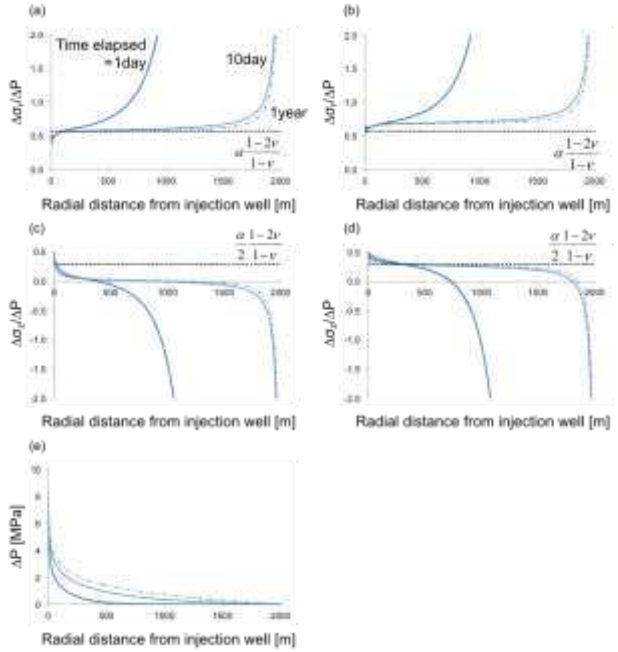

Figure 2. Spatio-temporal evolution of stress/pore-pressure change ratios when the hydraulic boundary of injection layer is open. (a) $\Delta\sigma_r/\Delta P$ at *middle* of injection layer, (b) $\Delta\sigma_r/\Delta P$ at *interface* between the injection layer and upper caprock, (c) $\Delta\sigma_z/\Delta P$ at *middle*, (d) $\Delta\sigma_z/\Delta P$ at *interface*, and (e) ΔP in the injection layer. Note: short-dashed line delineates the asymptotic values of $\Delta\sigma_r/\Delta P$ and $\Delta\sigma_z/\Delta P$ from the homogeneous infinite condition, respectively.

3.2 Permeability of Caprock

We conducted additional numerical experiments where the permeability of caprock is switched from k_{cap}=1 nd to k_{cap}=1 μd. We observed that both ratios $\Delta\sigma_r/\Delta P$ and $\Delta\sigma_z/\Delta P$ at the *middle* are barely affected by the change in the caprock permeability (Figures 4-a and c). However, the asymptote curves of these ratios at the *interface* shifted downward, to become similar with curves for the *middle* of injection zone (Figures 4-b and d). Therefore, we can ascertain that the permeability contrast indeed contributes to larger values of $\Delta\sigma/\Delta P$ at *the interface* comparing with those inside of the injection zone.

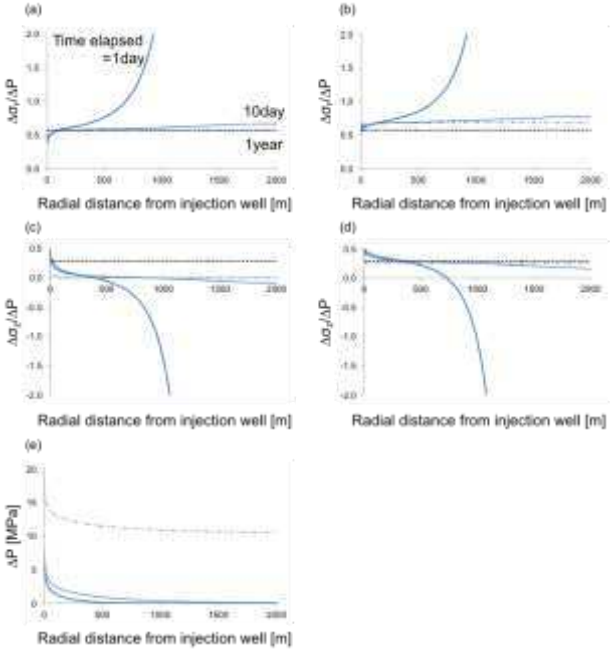

Figure 3. Spatio-temporal evolution of stress/pore-pressure change ratios when the hydraulic boundary of injection layer is closed. (a) $\Delta\sigma_r/\Delta P$ at *middle*, (b) $\Delta\sigma_r/\Delta P$ at *interface*, (c) $\Delta\sigma_z/\Delta P$ at *middle*, (d) $\Delta\sigma_z/\Delta P$ at *interface*, and (e) ΔP in the injection layer.

3.3 Implications on CO_2 Geologic Storage

Reactivation of pre-existing fractures via shear slip (i.e., induced seismic events) determines the maximum sustainable pressure limit because, in most cases, such reactivation occurs prior to shear failures of intact rock or tensile fractures (Rutqvist et al., 2007, Rutqvist et al., 2008). Assuming that pre-existing fractures could exist at any point with an arbitrary orientation, the potential for the shear slip can be expressed in terms of effective principal stresses σ_1' and σ_3' using the Coulomb failure criterion (cohesion is assumed zero for pre-existing fractures):

$$\sigma_1' = q_{slip}\sigma_3' \tag{2}$$

Slope q_{slip} in Equation 2 is a function of friction angle ϕ:

$$q_{slip} = \left[(\tan^2\phi + 1)^{1/2} + \tan\phi\right]^2 \tag{3}$$

If we consider 30° for the friction angle, the slope becomes q_{slip}=3. In traditional approaches, effective stress σ' is computed simply as a function of initial total stress σ_0, pore pressure $P=P_0+\Delta P$, and Biot's coefficient α: $\sigma' \fallingdotseq \sigma_0 - \alpha(P_0+\Delta P)$ (Guéguen and Boutéca, 2004). However, if we account for the pore-pressure/stress coupling effect, vertical and horizontal effective stresses, σ_v' and σ_h', can be updated as follows:

$$\sigma_v' = \sigma_{v0} + \beta_v \cdot \Delta P - \alpha \cdot \left(P_0 + \Delta P\right) \tag{4}$$

$$\sigma_h' = \sigma_{h0} + \beta_h \cdot \Delta P - \alpha \cdot \left(P_0 + \Delta P\right) \tag{5}$$

where $\beta_v = \Delta\sigma_v/\Delta P$ denotes the ratio of change in total vertical stress to change in pore pressure and $\beta_h = \Delta\sigma_h/\Delta P$ the ratio of change in total horizontal stress to change in pore pressure. Simplified poroelastic analysis has considered only $\beta_h = \Delta\sigma_h/\Delta P$ (i.e., β_v is assumed zero, $\Delta\sigma_v/\Delta P$=0) for estimating maximum sustainable pressure limit, which can be valid only for a thin, laterally extensive reservoir (Segall and Fitzgerald, 1998).

Rutqvist et al. observed that the traditional approach underestimates the pressure limit, whereas the simplified poroelastic analysis grossly overestimates the pressure limit for a case of normal-faulting stress regime (Rutqvist et al., 2007). Therefore, we should account for both β_h and β_v when attempting to evaluate an approximate value of maximum sustainable pressure limit quickly via the analytic computation. Moreover, the coupling ratios, β_h and β_v, need to be properly identified a priori given that the pore pressure is anticipated to increase during the CO_2 injection into a storage reservoir.

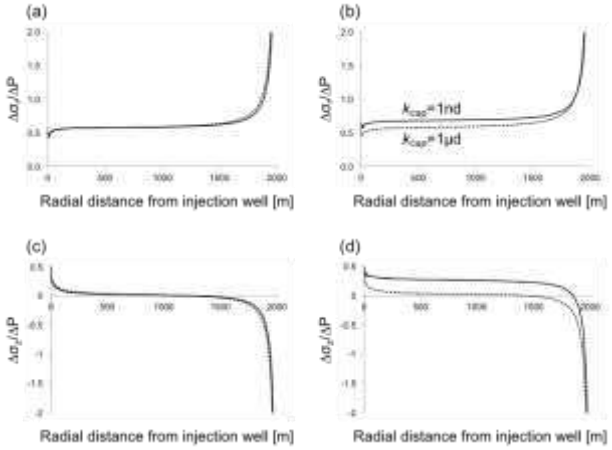

Figure 4. Spatial evolution of stress/pore-pressure change ratios with different caprock permeability k_{cap}. (a) $\Delta\sigma_r/\Delta P$ at *middle*, (b) $\Delta\sigma_r/\Delta P$ at *interface*, (c) $\Delta\sigma_z/\Delta P$ at *middle*, and (d) $\Delta\sigma_z/\Delta P$ at *interface*. Note: solid line represents when k_{cap}=1 nd, and dashed line represents when k_{cap}=1 μd.

4 CONCLUSION

Success of CO_2 geologic storage requires the precise prediction of reservoir stress paths during fluid injection. We conducted numerical experiments to investigate the spatio-temporal evolution of the ratios of change in total stress to change in pore-pressure $\Delta\sigma/\Delta P$ during fluid injection for different hydraulic boundary and caprock permeability conditions. Salient observations and suggestion follow.

The asymptotic value of $\Delta\sigma_r/\Delta P$ at the *interface* between the injection layer and upper caprock is greater than that at the *middle* of injection layer by 10-15%, caused by the significant permeability contrast. A broad area at the *interface* converges to $\Delta\sigma_z/\Delta P \approx (\alpha/2)(1\text{-}2\nu)/(1\text{-}\nu)$, while the *middle* line converges to $\Delta\sigma_z/\Delta P \approx 0$. Therefore, neglecting the vertical stress change is valid only for the inside of injection layer. All these ratios eventually converge to their asymptote curves, which become flat when the hydraulic boundary of injection layer is switched to closed.

We suggest taking the pore-pressure/stress coupling effect into consideration when attempting to evaluate stress paths and thus to determine the maximum sustainable pressure limit. While the traditional approach or the simplified poroelastic analysis would underestimate or overestimate the pressure limit, accurate reflection of the stress/pore-pressure change ratios can provide a reliable estimate of the maximum sustainable pressure limit.

5 ACKNOWLEDGEMENTS

Support for this research was provided by the Gulf Coast Carbon Center at the Bureau of Economic Geology (BEG) and the U.S. Department of Energy, NETL, under contract numbers DE-FE0009301 and DE-FC26-05NT42590. Any opinions, findings, conclusions, or recommendations expressed herein are those of the authors and do not necessarily reflect the views of the funding organizations.

6 REFERENCES

Altmann, J. B., Müller, T. M., Müller, B. I., Tingay, M. R., and Heidbach, O. 2010. Poroelastic contribution to the reservoir stress path. *International Journal of Rock Mechanics and Mining Sciences* 47 (7), 1104-1113.

Guéguen, Y. and Boutéca, M. 2004. *Mechanics of fluid saturated rocks*, Academic Press.

IPCC. 2005. *IPCC special report on carbon dioxide capture and storage*. Prepared by working group III of the intergovernmental panal on climate change, B. Metz, O. Davidson, H. C. de Coninck, M. Loos, and L. A. Meyer, ed., Cambridge University Press, Cambridge, United Kingdom and New York, USA, 442.

Kim, S. and Hosseini, S. 2015. Hydro-thermo-mechanical analysis during injection of cold fluid into a geologic formation. *International Journal of Rock Mechanics and Mining Sciences* 77, 220-236.

Preisig, M. and Prévost, J. H. 2011. Coupled multi-phase thermo-poromechanical effects. Case study: CO_2 injection at In Salah, Algeria. *International Journal of Greenhouse Gas Control* 5 (4), 1055-1064.

Rutqvist, J. 2012. The geomechanics of CO_2 storage in deep sedimentary formations. *Geotechnical and Geological Engineering* 30 (3), 525-551.

Rutqvist, J., Birkholzer, J., Cappa, F., and Tsang, C. F. 2007. Estimating maximum sustainable injection pressure during geological sequestration of CO_2 using coupled fluid flow and geomechanical fault-slip analysis. *Energy Conversion and Management* 48 (6), 1798-1807.

Rutqvist, J., Birkholzer, J., and Tsang, C. F. 2008. Coupled reservoir–geomechanical analysis of the potential for tensile and shear failure associated with CO_2 injection in multilayered reservoir–caprock systems. *International Journal of Rock Mechanics and Mining Sciences* 45 (2), 132-143.

Safari, M. R., Trevor, O., Queena, C., Hamed, C., Blair, N., Uno, M., and Hawkes, C. 2013. Effects of depletion/injection induced stress changes on natural fracture reactivation. Proc., *47th US Rock Mechanics/Geomechanics Symposium*, American Rock Mechanics Association, ARMA 13-395.

Schoenball, M., Müller, T., Müller, B., and Heidbach, O. 2010. Fluid-induced microseismicity in pre-stressed rock masses. *Geophysical Journal International* 180 (2), 813-819.

Segall, P. and Fitzgerald, S. D. 1998. A note on induced stress changes in hydrocarbon and geothermal reservoirs. *Tectonophysics* 289 (1), 117-128.

Socolow, R. H. and Pacala, S. W. 2006. A plan to keep carbon in check. *Scientific American* 295 (3), 50-57.

Vilarrasa, V., Carrera, J., and Olivella, S. 2013. Hydromechanical characterization of CO_2 injection sites. *International Journal of Greenhouse Gas Control* 19, 665-677.

Vilarrasa, V., Silva, O., Carrera, J., and Olivella, S. 2013. Liquid CO_2 injection for geological storage in deep saline aquifers. *International Journal of Greenhouse Gas Control* 14, 84-96.